# Amplitude-Aided CPHD Filter for Multitarget Tracking in Infrared Images

**Changzhen Qiu\*, Zhiyong Zhang, Huanzhang Lu, and Yabei Wu**

**Abstract**—The cardinalized probability hypothesis density (CPHD) filter is a powerful tool for multitarget tracking (MTT). However, conventional CPHD filter discriminates targets from clutter only via the motion information, which is not reasonable in the situation of dense clutter. In the tracking, the amplitude of target returns is usually stronger than those coming from clutter, so the amplitude information can be used to enhance the discrimination between targets and clutter. Based on this idea, this paper proposes an amplitude-aided CPHD filter for the MTT in distant infrared (IR) surveillance. First, we model the amplitude of targets and clutter in IR scenarios respectively. For distant IR scenarios, the point spread function (PSF) is used to model the imaging of the point target. The center intensity of the PSF is unknown in practice, and the maximum likelihood estimation (MLE) method is adopted to estimate the target center intensity via the intensities of the latest target detections. Then a likelihood function for MTT is established, and using this likelihood function, a new CPHD recursion is derived, which can distinguish different targets and clutter by the correspondence weight. In the implementation, we adopt the Gaussian mixture (GM) approach to implement the amplitude-aided CPHD filter to achieve efficient performance. In numerical experiments, the results show that the proposed method attains a significant improvement in performance over that only using location measurements.

## 1. INTRODUCTION

Infrared (IR) sensor has several outstanding advantages, high sensitivity, day and night working, and far working range. So it plays an important role in distant-target surveillance applications, especially in military community. For instances, the IR search and track (IRST) systems [1] are mounted on the military combat equipments and are used to search and lock the aircrafts in the surveillance air and provide fire control for the weapon systems. In the space-based IR system (SBIRS) [2], the IR sensors are used to search aircrafts and missiles in the space for early strategic warning. The IR sensor can also be used for the guidance of ballistic missile [3] by centering the target in the field of view (FOV).

In the information process of IR images, the extraction of high-level information mainly relies on the analysis of target trajectories, which are generated via multitarget tracking (MTT) techniques. MTT aims to simultaneously estimate the varying number of targets and their states from a sequence of observation sets. In the situation of large sensor-target distance, targets appear to be dim points in IR image, which means that a target occupies only a few pixels and lacks information of texture and spatial distribution. The signals of point targets will change according to the sensor-target distance, and they tend to be deteriorated by complex environment and noise. To address the MTT problems for dim point targets, track-before-detect (TBD) methods have been proposed to improve the tracking performance, especially under low signal-to-noise ratio (SNR) conditions [4, 5]. The TBD methods use whole raw image data as input data for tacking. The advantage is that it can make use of all information

contained in the images, but it is at the cost of drastic complexity increase. The TBD algorithms are too expensive for IR applications, in which the pixels amount is extraordinary large (e.g., 256 pix × 256 pix array). In scenarios of strong SNR, detect-before-track (DBT) methods are more tractable and real-time approaches. In the DBT scheme, a set of detections are firstly produced from the raw sensor returns, and then the detections are fed into the tracking algorithms. The detection step compresses the information of the image into a finite set of points, which it is efficient in terms of computational requirements [4].

Even under the assumption of strong SNR, the detection results in IR image still contain uncertain clutter and misdetections. The main reason is device system noise and environment surrounding, which are collectively referred as background noise in this paper. Involving the imperfect detections, a critical problem arising is that the associations between the detections and tracks are uncertain, i.e., it is not clear a priori which detection corresponds to the interested target or clutter. Data association is a burdensome problem especially under uncertain clutter and misdetections, and it is the main reason that leads to the complexity of MTT.

The common idea of traditional approaches is dividing the MTT problem into two sub-problems, data association and state estimation, i.e., firstly determines the association between detections and target tracks, and then estimates the state of each target separately. The data association methods are the core problems in traditional MTT. The most well-known data association methods include joint probabilistic data association (JPDA) [6] and multiple hypotheses tracking (MHT) [7]. The methods that have been developed for MTT in IR images include nearest neighbor (NN) [8], neural-network-based method [9], probabilistic multiple hypothesis tracking (PMHT) method [10, 11], and Markov random field (MRF) method [12]. However, computational complexity and associating performance are two conflicted aspects, so we do not expect to find data association algorithms that are efficient and exact.

Recently, finite sets statistics (FISST) is proposed by Mahler as a new tool for MTT [13]. FISST describes multitarget state by random finite set (RFS), and MTT can be unified to Bayesian framework and avoids the cumbersome data association. In the realization of Bayesian multitarget recursion, the sub-optimal solutions with first-order moment and second-order moment approximate is derived, resulting in probability hypothesis density (PHD) filtering [13] and cardinalized PHD (CPHD) filtering [14]. The PHD filtering propagates intensity of multitarget state, while the CPHD filtering propagates both intensity and cardinality distribution. The CPHD filter obtains more accurate estimations, and it has advantage in the situations of large target number and high clutter density, but it is at the cost of complexity increase which is cubic complexity in the number of measurements [15]. In addition to the PHD/CPHD filters, the multitarget multi-Bernoulli (MeMBer) filter proposed by Mahler [16] is an alternative approximation to the Bayesian multitarget recursion. Unlike the PHD/CPHD recursions, which propagate moments and cardinality distributions, the MeMBer recursion propagates the multitarget posterior density approximately. In the original MeMBer filtering, cardinality bias occurs in the data update step without considering cardinality distribution. Vo et al. developed a cardinality-balanced MeMBer (CBMeMBer) filter [17], which can reduce the cardinality bias by propagating a parameterized approximation to the posterior cardinality distribution. But the approximation of CBMeMBer filter is reasonable when clutter is not too dense, and the probability of detection is high.

Both traditional and FISST-based algorithms suppress the disturbance of clutter via target motion model in their original formulations. They are reasonable when the targets and clutter are sparse and well-separated. But in the situation of large target number and dense clutter, this method deteriorates and often leads to false tracks. Taking into account that the target returns are usually stronger than those of clutter, the amplitude information can be used to enhance the discrimination of the targets and clutter. The idea of using amplitude for target tracking has been proposed in the literature. For examples, Lerro and Bar-Shalom [18] proposed to use amplitude likelihood for probabilistic data association (PDA) and assign the measurements more similar to the target amplitude with larger association probability, so it can track single target more robust in dense clutter. Brekke et al. [19, 20] proposed a new conservative amplitude likelihood for the PDA filter with improved robustness, which attempted to detect and track moderately observable targets such as small boats or human divers in environments. Van Keuk [21] used amplitude information in MHT to improve the performance of MTT. For MTT approaches in the framework of FISST, Xu et al. [22] proposed a method which involves using

amplitude information in PHD filter to improve MTT performance, while Clark et al. [23] illustrated an approach using the target amplitude for both the PHD and CPHD filters.

In this paper, we adopt the CPHD filter for the MTT issue in distant IR surveillance, expecting accurate performance in the situations of large target number and high clutter density. Based on the CPHD filtering framework, we propose an amplitude-aided tracking method to improve the tracking performance. First, we model the amplitude of targets and clutter in IR scenarios respectively. For IR images target, the point spread function (PSF) is used to model the imaging of point target. In practice, the value of target center intensity is unknown, and the maximum likelihood estimation (MLE) method is proposed to estimate the target center intensity via the intensities of the latest target detections, which have been tracked by the tracker. Then a likelihood function for MTT is established, and using this likelihood function, a new CPHD recursion is derived, which can distinguish different targets and clutter by the correspondence weight. In the implementation, we adopt the Gaussian mixture (GM) approach to implement the amplitude-aided CPHD filter to achieve efficient performance. In numerical experiments, the results show that the proposed method attains a significant improvement in performance over just using location measurements.

The rest of this paper is organized as follows. In Section 2, the amplitude models for clutter and target in IR images are established. The proposed amplitude-aided GM-CPHD filtering is illustrated in Section 3. Section 4 verifies the proposed GM-CPHD filtering based on numerical simulation, and conclusions are drawn in Section 5.

## 2. AMPLITUDE MODELS FOR TARGET AND CLUTTER

In IR image-based tracking, a thresholding method is usually operated to obtain target detections. Due to background noise, the detections include actual targets and clutter (false alarms). In this section, we establish imaging models for IR point targets and clutter respectively. The target center intensity is unknown in practice, so the maximum likelihood estimation (MLE) method is proposed to estimate the target center intensity via the intensities of the latest detections.

### 2.1. Imaging Models of IR Sensor

In IR imaging, a so-called uniformity phenomenon exists in raw IR background image [24], and the non-uniformity correction technique is usually operated to improve the image quality. After non-uniformity correction, the intensity $a$ of the background noise is Gaussian distributed approximately [25]. Hence, the probability densities $p_0(a)$ for the intensity of background noise can be modeled by

$$p_0(a) = \frac{1}{\sqrt{2\pi}\sigma_I} \exp\left(-\frac{(a - \bar{I})^2}{2\sigma_I^2}\right) \tag{1}$$

where $\bar{I}$ and $\sigma_I^2$ are the mean and variance of the collected IR image respectively, and $\bar{I}$ and $\sigma_I^2$ mainly depend on the system noise level and environment radiation.

In distant surveillance, the range between targets and the sensor is large, so targets are point thermal sources for the IR imaging plane. The point target imaging suffers diffusion due to the diffraction effect of optical system. An important concept to describe imaging diffusion is the point spread function (PSF). If the two dimensions of the imaging plane are denoted as $r$ axis and $c$ axis, then a typical PSF $s(r, c)$ for IR target is given as [26]

$$s(r, c) = A \exp\left\{-\frac{[(r - r_0)]^2}{2\sigma_r^2} - \frac{[(c - c_0)]^2}{2\sigma_c^2}\right\} \tag{2}$$

where $(r_0, c_0)$ is the target center position, $A$ the center intensity of the target signal, and $\sigma_r$ and $\sigma_c$ are the diffusion coefficients along $r$ axis and $c$ axis, respectively.

The target intensities are cumulated to the background noise additively [27]. If a pixel $(r, c)$ is illuminated by a target center at $(r_0, c_0)$, then the probability density of intensity $a$ of the pixel $(r, c)$ is also Gaussian distributed, and can be modeled by

$$p_1(a|s(r, c)) = \frac{1}{\sqrt{2\pi}\sigma_I} \exp\left(-\frac{(a - \bar{I} - s(r, c))^2}{2\sigma_I^2}\right) \tag{3}$$
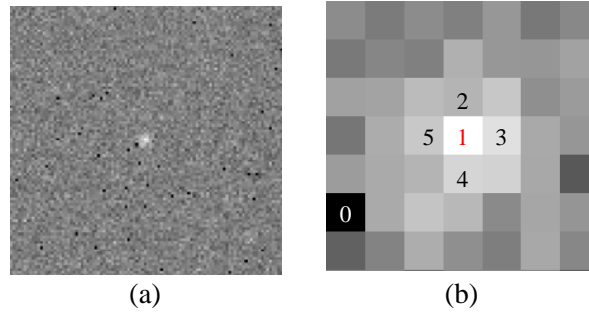
**Figure 1.** Snapshots of IR image. (a) Original target image. (b) Zoom target image.

Specially, the probability density of the target center intensity is modeled by

$$p_1(a|s(r_0, c_0)) = \frac{1}{\sqrt{2\pi}\sigma_I} \exp\left(-\frac{(a - \bar{I} - A)^2}{2\sigma_I^2}\right) \tag{4}$$

A snapshot of the IR target image is shown in Figure 1(a), and Figure 1(b) is the zoom image of the target. The amplitude is assumed to be identical for each target. If regions of the targets on the image overlap, then their intensities are cumulated additively.

Another special reason to cause misdetections is the existences of defect-pixels in the IR imaging plane. In manufacturing, the IR imaging plane array (for example, staring IR focal plane array) inevitably suffers from defect-pixels due to the limit of technical level. The amplitude of a defect-pixel is in a high level and changes randomly. In engineering practice, the defect-pixels are tested offline and are fixed on a small value in order to depress their disturbance for tracking. A defect-pixel appears to be a black spot just as the pixel labeled by 0 in Figure 1(b).

## 2.2. Estimation of Target Center Intensity

In practice, the target center intensity $A$ is unknown, and $A$ depends on the target temperature and working range. Considering that the frame rate of IR sensor is quite high, so during a small time moment, the target center intensity can be deemed unchanged. In other words, $A$ can be assumed unaltered during the latest $L_{Fr}$ frames data. The intensities of the latest detections imply the information of target amplitude. Based on this idea, we derive a method to estimate $A$ via the previous target detections.

In the detection step, a thresholding method is used for point target detection commonly, and the segmentation threshold $\tau_D$ is usually defined as

$$\tau_D = \bar{I} + k_s\sqrt{\sigma_I} \tag{5}$$

where $\bar{I}$ and $\sigma_I^2$ are the mean and variance of the IR image respectively, and $k_s$ is the segmentation coefficient.

After the thresholding operation, a connected components labeling algorithm is adopted to extract pixels belonging to the targets [28]. A connected component illuminated by the target with state $x$ is denoted by $T(x)$. For each connected component $T_i(x)$, we deem that the strongest intensity $a_i$ in $T_i(x)$ is a measurement of the target center intensity. Although the strongest intensity $a_i$ may correspond to the surrounding pixels due to background noise, and such an approximate processing is reasonable because the generating error is acceptable. If the number of connected components that have been tracked by the tracker in the latest $L_{Fr}$ frames is $n$, then we can form the measurements of target center intensity in the latest $L_{Fr}$ frames as a vector $A_D = [a_1, \ldots, a_n]$. The value of $L_{Fr}$ depends on the practical frame rate, insuring that the algorithm can utilize detections as much as possible and also keep the unaltered characteristic of the target amplitude.

Notice that all values in $A_D = [a_1, \ldots, a_n]$ are above $\tau_D$, and they do not obey the model in (4). Let $Z$ be the distribution space of target center intensity and $P(\cdot)$ the event probability, then a value $a$ in $A_D$ is a conditional probability on $Z$ with the condition $a > \tau_D$. And the probability mass function

$F(a)$ of $a$ is

$$F(a) = P\left(\bar{\underline{Z}} \le a | \bar{\underline{Z}} \ge \tau_D\right) = \frac{P\left(\tau_D \le \bar{\underline{Z}} \le a\right)}{P\left(\bar{\underline{Z}} \le \tau_D\right)} = \frac{\phi_1(a) - \phi_1(\tau_D)}{\phi_1(\tau_D)} = \frac{\phi_1(a)}{\phi_1(\tau_D)} - 1 \tag{6}$$

where $\bar{\underline{Z}}$ denotes a sample in $Z$, and $\phi_1(\cdot)$ is probability mass function corresponding to (4). Differentiating (6) and substituting (4) into the result yields the probability density function $f(z)$ as

$$f(a) = \frac{\partial F(a)}{\partial a} = \frac{1}{\phi_1(\tau_D)} \frac{1}{\sqrt{2\pi}\sigma_I} \exp\left(-\frac{(a - (\bar{I} + A))^2}{2\sigma_I^2}\right) \tag{7}$$

where

$$\phi_1(\tau_D) = \int_{-\infty}^{\tau_D} \frac{1}{\sqrt{2\pi}\sigma_I} \exp\left(-\frac{(a - (\bar{I} + A))^2}{2\sigma_I^2}\right) da \tag{8}$$

Now the problem is to estimate $A$ in (7) with the sample set $A_D = [a_1, \ldots, a_n]$. Let $\theta = \bar{I} + A$, and we employ the MLE method [29] to estimate $\theta = \bar{I} + A$. With the assumption that the measurements in $A_D = [z_1, \ldots, z_n]$ are independent, the likelihood function is constructed as

$$L = \frac{1}{\phi_1^n(\tau_D; \theta)} \frac{1}{\left(\sqrt{2\pi}\right)^n \sigma_I^n} \exp\left(-\frac{\sum_{i=1}^{n} (a_i - \theta)^2}{2\sigma_I^2}\right) \tag{9}$$

Differentiating the log-likelihood function and setting it equal to zero, we have

$$\frac{\bar{a} - \theta}{\sigma_I^2} \phi_1(\tau_D; \theta) - \frac{1}{\sqrt{2\pi}\sigma_I} \exp\left(-\frac{(\tau_D - \theta)^2}{2\sigma_I^2}\right) = 0 \tag{10}$$

where $\bar{a} = \frac{1}{n} \sum_{i=1}^{n} a_i$. We approximate (10) by first-order Taylor series at $\theta = \bar{I} + A$, then the solution of $\hat{\theta}$ is obtained. The final estimation of $A$ is

$$\hat{A} = \bar{a} - \bar{I} - \frac{\sigma_I^2}{\bar{a} - \tau_D + \exp\left(\frac{(\tau_D - \bar{a})^2}{2\sigma_I^2}\right) \int_{-\infty}^{\tau_D} \exp\left(\frac{-(a - \bar{a})^2}{2\sigma_I^2}\right) da} \tag{11}$$

Equation (11) does not contain unknown parameter, so it can be calculated using numerical methods.

## 3. AMPLITUDE-AIDED GM-CPHD TRACKER

In this section, we incorporate the amplitude information to the prediction and update equations of original CPHD filter to enhance the discrimination between targets and false alarms. Also, the GM implementation of the new CPHD tracker is given.

### 3.1. Conventional CPHD Recursion

Based on the RFS framework, the multitarget tracking can be unified to Bayesian framework rigorously. Suppose that at moment $k$, there are $N(k)$ targets with states $x_{k,1}, \ldots, x_{k,N(k)}$ and each taking values in a state space $\mathcal{X}$ and that $M(k)$ observations $z_{k,1}, \ldots, z_{k,M(k)}$ are received and each taking values in an observation space $\mathcal{Z}$. Then, the multitarget state $X_k$ and multitarget observation $Z_k$ are defined as $X_k = \{x_{k,1}, \ldots, x_{k,N(k)}\} \in \mathcal{F}(\mathcal{X})$, $Z_k = \{z_{k,1}, \ldots, z_{k,M(k)}\} \in \mathcal{F}(\mathcal{Z})$, where $\mathcal{F}(\mathcal{X})$ and $\mathcal{F}(\mathcal{Z})$ denote the respective collections of all finite subsets [30] of $\mathcal{X}$ and $\mathcal{Z}$.

Using the FISST, Mahler derived the second-order approximate of the optimal Bayesian filtering, which results in the CPHD filter [31]. Similar to typical Bayesian filtering, the CPHD filter also involves two steps, prediction and update. For simplicity, we do not consider target spawning in this paper.

### 3.1.1. Prediction

Suppose that at moment $k-1$, the posterior intensity $v_{k-1}(x)$ and posterior cardinality distribution $\rho_{k-1}$ are given, then the predicted cardinality distribution $\rho_{k|k-1}$ and predicted intensity $v_{k|k-1}$ are given by

$$\rho_{k|k-1}(n) = \sum_{j=0}^{n} \rho_{\Gamma,k}(n-j)\Pi_{k|k-1}\left[v_{k-1}, \rho_{k-1}\right](j) \tag{12}$$

$$v_{k|k-1}(x) = \gamma_k(x) + \int p_{S,k}\left(x'\right) f_{k|k-1}(x|x')v_{k-1}\left(x'\right) dx' \tag{13}$$

where

$$\Pi_{k|k-1}\left[v, \rho\right](j) = \sum_{l=j}^{\infty} C_j^l \frac{\langle \rho_{S,k}, v\rangle^j \langle 1 - \rho_{S,k}, v\rangle^{l-j}}{\langle 1, v\rangle^l}\rho(l) \tag{14}$$

and $\rho_{\Gamma,k}(\cdot)$ is the cardinality distribution of birth RFS, $\gamma_k(\cdot)$ the intensity function of birth RFS, $p_{S,k}(x')$ the probability of target survival, and $f_{k|k-1}(x|x')$ the single target Markov transition density from $k-1$ to time $k$.

### 3.1.2. Update

If at time $k$, the predicted cardinality distribution $\rho_{k|k-1}$ and predicted intensity $v_{k|k-1}$ are given, then for a given measurement set $Z_k$, the updated cardinality distribution $\rho_k$ and updated intensity $v_k$ are given by

$$\rho_k(n) = \frac{\Upsilon_k^0\left[v_{k|k-1}, Z_k\right](n)\rho_{k|k-1}(n)}{\left\langle \Upsilon_k^0\left[v_{k|k-1}, Z_k\right], \rho_{k|k-1}\right\rangle} \tag{15}$$

$$v_k(x) = v_{k|k-1}(x)\left[\frac{\left\langle \Upsilon_k^1\left[v_{k|k-1}; Z_k\right], \rho_{k|k-1}\right\rangle}{\left\langle \Upsilon_k^0\left[v_{k|k-1}; Z_k\right], \rho_{k|k-1}\right\rangle}(1 - p_{D,k}(x)) + \sum_{z \in Z_k}\Psi_{k,z}(x)\frac{\left\langle \Upsilon_k^1\left[v_{k|k-1}; Z_k - \{z\}\right], \rho_{k|k-1}\right\rangle}{\left\langle \Upsilon_k^0\left[v_{k|k-1}; Z_k\right], \rho_{k|k-1}\right\rangle}\right] \tag{16}$$

where

$$\Upsilon_k^u\left[v, Z\right](n) \equiv \sum_{j=0}^{\min(|Z|,n)}(|Z|-j)! \cdot \rho_{K,k}(|Z|-j)P_{j+u}^n\frac{\langle 1 - p_{D,k}(x), v\rangle^{n-(j+u)}}{\langle 1, v\rangle^n} \cdot e_j\left(\Xi_k(v, Z)\right) \tag{17}$$

$$\Xi_k(v, Z) = \{\langle v, \Psi_{k,z}\rangle : z \in Z\} \tag{18}$$

$$\Psi_{k,z}(x) = \frac{\langle 1, \kappa_k\rangle}{\kappa_k(z)}g_k(z|x)p_{D,k}(x) \tag{19}$$

and $p_{D,k}(x)$ is the detection probability of state at time $k$, $g_k(z|x)$ the single target measurement likelihood at time $k$, $\rho_{K,k}(\cdot)$ the cardinality distribution of clutter RFS at time $k$, and $\kappa_k(\cdot)$ the intensity function of clutter RFS at time $k$.

## 3.2. Amplitude-Aided Likelihood and Detection Probability Estimation

The amplitude information can incorporate to the likelihood function of the filter to enhance the performance. We assume that the amplitude of the signal return is independent of target state location, and thus the amplitude-aid likelihoods for targets $g'(z|x)$ and the likelihood $c'(z)$ for clutter are given by

$$g'(z|x) = g(z|x)g_a^{\tau_D}\left(a|E_R\right) \tag{20}$$

$$c'(z) = c(z)c_a^{\tau_D}(a) \tag{21}$$

where $g(z|x)$ and $c(z)$ are the original likelihood function of target and clutter respectively [32], and $c_a^{\tau_D}(a)$ and $g_z^{\tau_D}(a|E_R)$ are the amplitude likelihood functions for the false alarm and the target, respectively, and

$$c_a^{\tau_D}(a) = \frac{1}{p_{FA}^{\tau_D}}p_0(a), \quad a > \tau_D \tag{22}$$

$$g_z^{\tau_D}(a|E_R) = \frac{1}{p_D^{\tau_D}(A)}p_1(a|A), \quad a > \tau_D \tag{23}$$

where $p_{FA}^{\tau_D}$ and $p_D^{\tau_D}$ are the detection probabilities of clutter and target. Based on (1), with a threshold $\tau_D$, $p_{FA}^{\tau_D}$ can be calculated by

$$p_{FA}^{\tau_D} = \int_{\tau_D}^{\infty} p_0(a)da = erf((\tau_D - \bar{I})/\sigma) \tag{24}$$

where $erf(x) = \frac{1}{\sqrt{2\pi}}\int_x^{+\infty}\exp(-\frac{y^2}{2})dy$ is the probability error function.

The detection probability $p_D^{\tau_D}(A)$ is unknown in practice. In theory, all pixels in the target region will contribute to the target detection. In dim IR target scenarios, we deem that only the central 5 pixels, which are labeled by numbers 1~5 in Figure 1(b), may contribute to the target detection. The reasons are two: i) according to the model in (3), the center pixels concentrate the majority energy of the target, and other pixels that away from the center receive little target energy spread; ii) only when all the central 5 pixels are miss-detected, the other pixels may contribute to the target detection, but the probability that all the 5 central pixels are miss-detected is very small.

With the above discussions, the target detection probability will be calculated by the central 5 pixels in the following. For each pixel $i$ with position $(r_i, c_i)$, the detection probability under the threshold $\tau_D$ is

$$\hat{P}d_i = \int_{\tau_D}^{\infty} \frac{1}{\sqrt{2\pi}\sigma_I}\exp\left(-\frac{(a - \bar{I} - s(r_i, c_i))^2}{2\sigma_I^2}\right)da \tag{25}$$

A target cannot be detected when it falls into a defect-pixel. Considering the influence of defect-pixels, the estimation is modified as

$$\hat{P}d_i' = \hat{P}d_i - \frac{N_F}{N_{col}N_{row}} \tag{26}$$

where $N_F$ is the number of defect-pixels and $N_{col}N_{row}$ the size of the IR pixel plane. Taking into account of the contribution of the central 5 pixels, the estimation of target detection probability is

$$P_D^{\tau_D} = \hat{P}d_1' + \left(1 - \hat{P}d_1'\right)\hat{P}d_2' + \left(1 - \hat{P}d_1'\right)\left(1 - \hat{P}d_2'\right)\hat{P}d_3' + \left(1 - \hat{P}d_1'\right)\left(1 - \hat{P}d_2'\right)\left(1 - \hat{P}d_3'\right)\hat{P}d_4'$$
$$+ \left(1 - \hat{P}d_1'\right)\left(1 - \hat{P}d_2'\right)\left(1 - \hat{P}d_3'\right)\left(1 - \hat{P}d_4'\right)\hat{P}d_5' \tag{27}$$

Assume that clutter distribute in the observation space uniformly, and the clutter intensity function $\kappa_k(z) = \lambda_c V c(z)$, where $\lambda_c$ is the clutter rate, $V$ the observation volume, and $c(z)$ the clutter probability density. So substituting (20)–(21) into (19) yields:

$$\Psi_{k,\tilde{z}}(x) = \frac{\int \lambda_c V c(z)c_a^{\tau}(a)dzda}{\lambda_c V c(z)c_a^{\tau}(a)} * g(z|x)g_a^{\tau_D}(a|A)p_D^{\tau_D}(A) \tag{28}$$

Substituting (24) and (27) into (28) yields:

$$\Psi_{k,z}(x) = \frac{g(z|x)g_a^{\tau_D}(a|E_R)p_D^{\tau_D}(A)}{c_z(z)c_a^{\tau}(a)} \tag{29}$$

Replace (19) of conventional recursion by (29), we obtain the new updated equation incorporated with amplitude information. Notice that the prediction equation of amplitude-aided CPHD filter is the same as standard CPHD filter.

### 3.3. The GM Implementation of Amplitude-Aided CPHD Recursion

The GM implementation of the amplitude-aided CPHD filter is based on the assumption that each actual target follows a linear Gaussian dynamical model, i.e.,

$$f_{k|k-1}^{(1)}(x|\zeta) = N(x; F_{k-1}\zeta, Q_{k-1}) \tag{30}$$

$$g_k(z|x) = N(z; H_k\zeta, R_k) \tag{31}$$

where $F_{k-1}$ is the state transition matrix, $Q_{k-1}$ the process noise covariance, $H_k$ the observation matrix, and $R_k$ the observation noise covariance. The survival and detection probabilities for actual targets are state independent. In addition, the intensity of the actual target birth RFS is a Gaussian mixture of the form

$$\gamma_k^{(1)}(x) = \sum_{i=1}^{J_{\gamma,k}} w_{\gamma,k}^{(i)} N\left(x; m_{\gamma,k}^{(i)}, P_{\gamma,k}^{(i)}\right) \tag{32}$$

where $J_{\gamma,k}, w_{\gamma,k}^{(i)}, m_{\gamma,k}^{(i)} P_{\gamma,k}^{(i)}, i = 1, \ldots, J_{\gamma,k}$ are given model parameters. Then, the prediction and update of GM implementation for amplitude-aided CPHD filtering with unknown clutter rate is as follows.

### 3.3.1. Prediction

Suppose that at moment $k-1$, the posterior intensity $v_{k-1}$ and posterior cardinality distribution $\rho_{k-1}$ are given, and $v_{k-1}(x)$ is given by

$$v_{k-1}(x) = \sum_{i=1}^{J_{k-1}} w_{k-1}^{(i)} \mathcal{N}\left(x; m_{k-1}^{(i)}, P_{k-1}^{(i)}\right) \tag{33}$$

Then the filtering prediction equation is

$$v_{k|k-1}(x) = p_{S,k} \times \sum_{j=1}^{J_{k-1}} w_{k-1}^{(j)} \mathcal{N}\left(x; m_{S,k|k-1}^{(j)}, P_{S,k|k-1}^{(j)}\right) + \gamma_k(x) \tag{34}$$

$$\rho_{k|k-1}(n) = \sum_{j=0}^{n} \rho_{\Gamma,k}(n-j) \sum_{l=j}^{\infty} C_j^l \rho_{k-1}(l)(1-p_{S,k})^{l-j} p_{S,k}^j \tag{35}$$

where the predict intensity $v_{k|k-1}$ is also Gaussian mixture, $C_j^l = l!/(j!(l-j)!)$ the binomial coefficient, and $P_j^n = n!/(n-j)!$ the permutation coefficient, and

$$m_{S,k|k-1}^{(j)} = F_{k-1} m_{k-1}^{(j)} \tag{36}$$

$$P_{S,k|k-1}^{(j)} = Q_{k-1} + F_{k-1} P_{k-1}^{(j)} F_{k-1}^T \tag{37}$$

### 3.3.2. Update

Suppose that at moment $k$, the predicted intensity $v_{k|k-1}$ and predicted cardinality distribution $\rho_{k|k-1}$ are given, and $v_{k|k-1}$ is a Gaussian mixture given by

$$v_{k|k-1}(x) = \sum_{i=1}^{J_{k|k-1}} w_{k|k-1}^{(i)} \times \mathcal{N}\left(x; m_{k|k-1}^{(i)}, P_{k|k-1}^{(i)}\right) \tag{38}$$

Then the updates for a given observation set $Z_k$ are given by

$$v_k(x) = (1-p_{D,x}) \frac{\left\langle \Psi_k^1[w_{k|k-1}, Z_k], \rho_{k|k-1}\right\rangle}{\left\langle \Psi_k^0\left[w_{k|k-1}, Z_k\right], \rho_{k|k-1}\right\rangle} v_{k|k-1}(x) + \sum_{z \in Z_k} \sum_{j=1}^{J_{k|k-1}} w_{D,k}^{(j)}(z) \mathcal{N}\left(x; m_k^{(j)}, P_k^{(j)}\right) \tag{39}$$

$$\rho_k(n) = \frac{\Psi_k^0\left[w_{k|k-1}, Z_k\right] \rho_{k|k-1}(n)}{\left\langle \Psi_k^0\left[w_{k|k-1}, Z_k\right], \rho_{k|k-1}\right\rangle} \tag{40}$$

where the update posterior intensity $v_k$ is also Gaussian mixture, $\langle \cdot, \cdot \rangle$ is the inner product defined between two real valued functions $\alpha$ and $\beta$ by $\langle \alpha, \beta \rangle = \sum_{l=0}^{\infty} \alpha(l)\beta(l)$, and

$$\Psi_k^u [w, Z](n) = \sum_{j=0}^{\min(|Z|,n)} (|Z| - j)p_{K,k}(|Z| - j)P_{j+u}^n \times \frac{(1 - p_{D,k})^{n-(j+u)}}{\langle 1, w \rangle^{j+u}} e_j \left( \Lambda_k(w, Z) \right) \tag{41}$$

$$\Lambda_k(w, Z) = \left\{ \frac{g_a^\tau(a|E_R)p_D^\tau(A)w^T q_k(z)}{c(z)c_a^{\tau_D}(a)} : z \in Z \right\} \tag{42}$$

$$w_{k|k-1} = \left[ w_{k|k-1}^{(1)}, \ldots, w_{k|k-1}^{(J_{k|k-1})} \right]^T \tag{43}$$

$$q_k(z) = \left[ q_k^{(1)}(z), \ldots, q_k^{(J_{k|k-1})}(z) \right]^T \tag{44}$$

$$q_k^{(j)}(z) = \mathcal{N} \left( z; H_k m_{k|k-1}^{(j)}, H_k P_{k|k-1}^{(j)} H_k^T + R_k \right) \tag{45}$$

$$w_k^{(j)}(z) = \frac{g_a^\tau(a|E_R)p_D^\tau(A)w_{k|k-1}^{(j)} q_k^{(j)}(z)}{c(z)c_a^{\tau_D}(a)} \times \frac{\left\langle \Psi_k^1 \left[ w_{k|k-1}, Z_k \backslash \{z\} \right], p_{k|k-1} \right\rangle}{\left\langle \Psi_k^0 \left[ w_{k|k-1}, Z_k \right], p_{k|k-1} \right\rangle} \tag{46}$$

$$m_k^{(j)}(z) = m_{k|k-1}^{(j)} + K_k^{(j)} \left( z - H_k m_{k|k-1}^{(j)} \right) \tag{47}$$

$$P_k^{(j)} = \left[ 1 - K_k^{(j)} H_k \right] P_{k|k-1}^{(j)} \tag{48}$$

$$K_k^{(j)} = P_{k|k-1}^{(j)} H_k^T \left[ H_k P_{k|k-1}^{(j)} H_k^T + R_k \right]^{-1} \tag{49}$$

In each prediction and update recursions, the mean target number is estimated as $\hat{N}_k^{(1)} = \sum_{j=1}^{J_k} w_k^{(i)}$. In addition, pruning and merging of Gaussian elements should also be considered, see [33] for more details.

## 4. SIMULATIONS

This section presents numerical studies for the proposed method. A linear Gaussian example is used to examine the performance of the proposed GM-CPHD-based tracker using amplitude features.

### 4.1. Scenario

In the numerical simulation, the observation image is a $N_{col} \times N_{row} = 256 \times 256$ array, and $1 \leq r \leq 256$, $1 \leq c \leq 256$. The observation model is based on (1)–(4). In (4), the target center intensity is time-varying with $A = 18 + 0.001t^2$, and $\sigma_r = \sigma_c = 1.5$. The mean and standard deviation of the image are $\bar{I} = 4000$ and $\sigma_I = 2.72$, respectively. Defect-pixels are also added to the observation image. We assume that the number of defect-pixels is $N_F = 1000$. All defect-pixels are set to 1, and they spread uniformly in the pixel plane.

Targets appear at the center of the field of view (FOV) and move constantly. The target velocity is measured in image pixel, and the single-target state space is modeled by the linear Gaussian in (30) and (31) with parameters

$$F_k = \begin{bmatrix} I_2 & \Delta I_2 \\ 0_2 & I_2 \end{bmatrix}; \quad Q_k = \sigma_v^2 \begin{bmatrix} \dfrac{\Delta^4}{4}I_2 & \dfrac{\Delta^3}{2}I_2 \\ \dfrac{\Delta^3}{2}I_2 & \Delta^2 I_2 \end{bmatrix}; \quad H_k = [I_2 \quad 0_2]; \quad R_k = \sigma_\varepsilon^2 I_2 \tag{50}$$

where $\Delta = 1\,\mathrm{s}$ is the sampling period, $I_n$ the unit matrix of $n \times n$, $0_n$ the zero matrix of $n \times n$, $\sigma_v = 0.01\,\mathrm{pixel/s^2}$ the standard deviation of state noise, and $\sigma_\varepsilon = 0.01\,\mathrm{pixel/s^2}$ the standard deviation of observation noise.

The maximum target number is 5, and the total time is 100 seconds in our simulation. The 5 targets' durations are $t_1 = 1 \sim 72$ s, $t_{2,3} = 20 \sim 84$ s, $t_{4,5} = 40 \sim 100$ s respectively, where the subscript denotes different targets. Newborn target RFS is Poisson distribution, with intensity of

$$\gamma_k^{(1)}(x) = \sum_{i=1}^{5} w_\gamma \mathcal{N}\left(x; m_\gamma^{(i)}, P_\gamma\right) \tag{51}$$

where $w_\gamma = 0.03$, and $m_\gamma^{(1)} = [0, 1.8, 0, 1.8]^T$; $m_\gamma^{(2)} = [0, -0.5, 0, -2]^T$; $m_\gamma^{(3)} = [0, 0.5, 0, 2]^T$; $m_\gamma^{(4)} = [0, 1.25, 0, -1.75]^T$; $m_\gamma^{(5)} = [0, -1.25, 0, 1.75]^T$. The demonstrations of IR image observations are shown in Figure 2.

The latest $L_{Fr} = 10$ frames are used to estimate the target center intensity, and in the first 10 frames, the filter is operated with $p_{D,0}^{(1)} = 0.8$. For the filter, the survival probability of targets is $p_{S,k}^{(1)} = 0.99$. The segment coefficient is set as $k_s = 4$, so the clutter rate is 10 for average. In Gaussian component pruning and merging, the weight threshold is $T' = 10^{-5}$, the combined threshold $U' = 4$ m, and the maximum number of Gaussian components $J_{\max} = 100$.

## 4.2. Results

To verify the performance of the proposed CPHD filter, 100 Monte Carlo runs are performed for the same scenario. The true and estimated target amplitudes are plotted in Figure 3(a), and Figure 3(b) is the standard deviation of amplitude estimation. The results show that the estimations of target amplitude are reasonable with an acceptable error. During the time $k < 20$, since only one target exists in the FOV. The target detections generated by the latest $L_{Fr}$ frames are limited, so $\hat{A}$ are estimated via small samples set, which leads to that the results suffer notable bias. When $k >= 20$, more targets
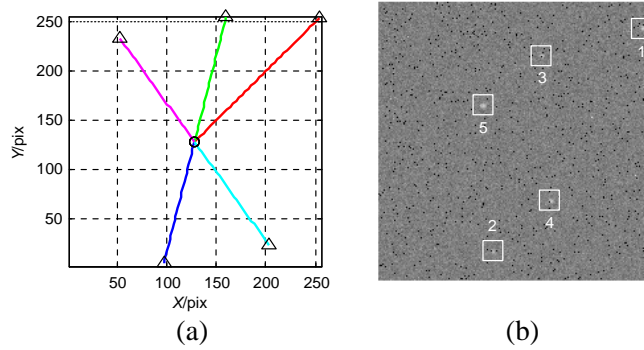


**Figure 2.** Target observations. (a) True target trajectories in the $xy$ plane, where start/stop positions for each track are shown with $O/\triangle$. (b) Snapshot of observations with 5 targets at time 65, the boxes indicate the target positions.
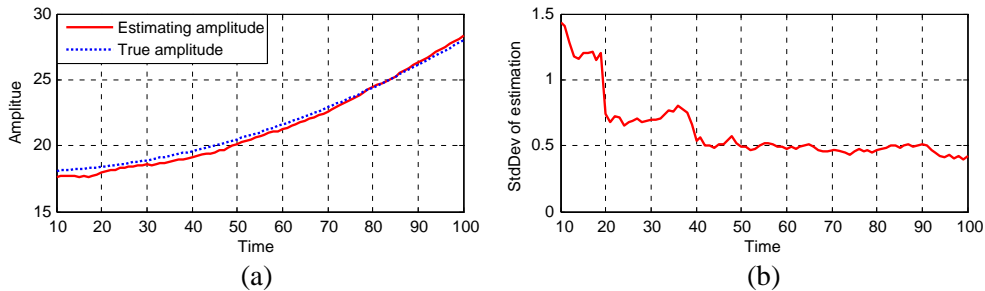


**Figure 3.** 100 Monte Carlo run average results. (a) True and estimated target amplitude. (b) The standard deviation of amplitude estimation.

exist in the FOV, and the number of target detections increases, then both the average estimation and the deviation decrease to more reasonable values. But estimations by the proposed method still exhibit uncertain bias. One main reason is that the samples set for target center intensity estimation may include some false tracks. However, the bias is slight, and we deem that it is in a reasonable scope. In practice, the sampling period of IR sensor is much less than $\Delta = 1\,\mathrm{s}$, and a higher data rate enables us to set $L_{Fr}$ on a larger value, which enables us to expect more exact estimation.

Under the target amplitude as $A = 18 + 0.001t^2$, the detection probability keeps altering all the time. The true detection probability $P_D(k)$ at each time $k$ is infeasible to obtain. We adopt an offline Monte Carlo estimation to approximate the true detection probability. After the 100 Monte Carlo runs, based on the prior scenarios parameters, we attain the number of real target states $M_x(k)$ and the number of target detections $M_D(k)$, then the Monte Carlo approximation of detection probability is

$$P_{MC}(k) = M_D(k)/M_x(k) \qquad (52)$$

The results of $P_{MC}(k)$ are shown in Figure 4(a). On the other hand, the detection probability estimation $\hat{P}_D(k)$ output by the tracker for 100 Monte Carlo run results is also computed. The average results and standard deviations are shown in Figures 4(a) and (b), respectively. We discard the first $L_{Fr} = 10$ frames where the detection probability is fixed to $p_{D,0}^{(1)} = 0.8$.

It can be seen that the estimations $\hat{P}_D(k)$ of the tracker and the statistic $P_{MC}(k)$ by Monte Carlo ascend similarly, especially in the latter part of the simulation when the target amplitude getting stronger. The estimation deviation of $\hat{P}_D(k)$ is similar to that of $\hat{A}$, and the reason is identical.

The outputs of CPHD filters with and without amplitude information for a single run are shown in Figure 5 and Figure 6, respectively. The plots give the $x$ and $y$ coordinates of the true and estimated positions, along with the $x$ and $y$ coordinates of the received measurements versus time. The figures show that the amplitude-aid CPHD filter can initiate and terminate each of the tracks better than that of conventional CPHD filter. Occasional incidences of false and dropped tracks are observed apparently in Figure 5 due to dense clutter, while in Figure 6, the proposed filter eliminates the influence of clutter based on the amplitude information, and the estimates of the target positions are markedly
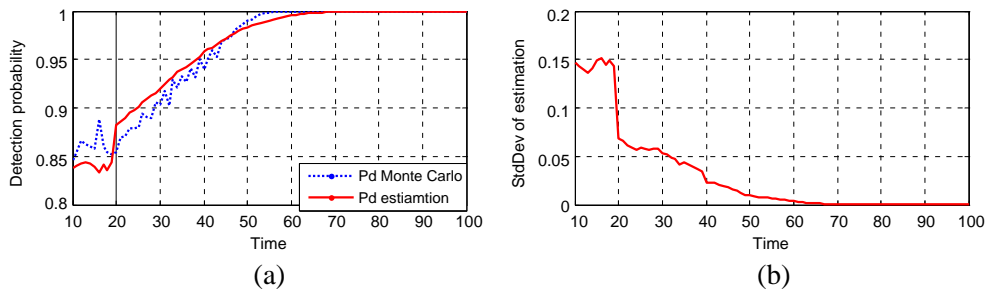


**Figure 4.** The 100 Monte Carlo run average results. (a) The average estimation of the Monte Carlo method and the proposed tracker. (b) The estimation standard deviation of the proposed tracker.
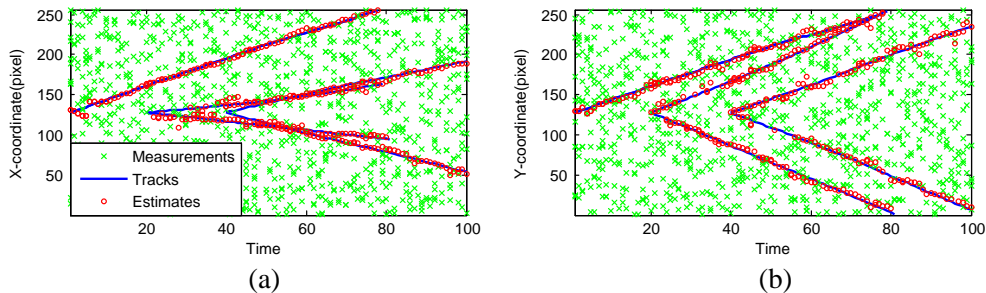


**Figure 5.** Estimates of the conventional CPHD filter and true tracks in $x$ and $y$ coordinates versus time.
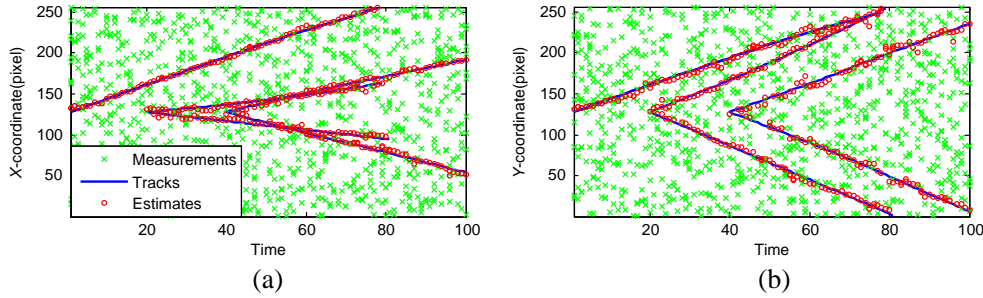
**Figure 6.** Estimates of the amplitude-aid CPHD filter and true tracks in $x$ and $y$ coordinates versus time.
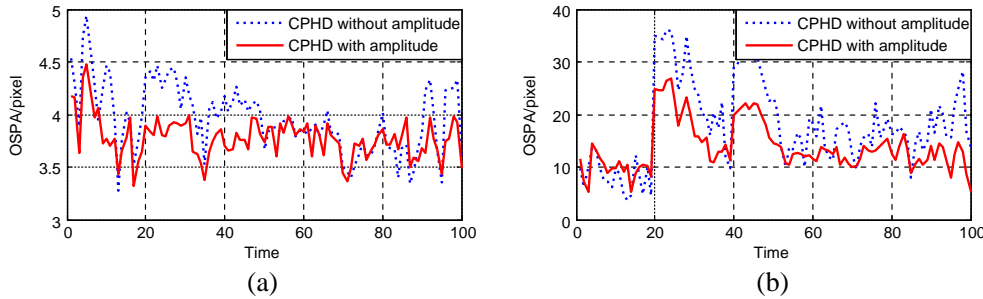


**Figure 7.** OSPA miss distance versus time for the conventional and amplitude-aid CPHD filters, (a) $p = 2$, $c = 5$, and (b) $p = 2$, $c = 50$.

more reasonable. However, a few of the false tracks still exist in the results. This is because our method is reasonable only under the condition that the amplitudes of the targets are stronger than that from clutters. But the clutters have comparable amplitudes to the targets under a certain probability. In this situation, our method fails to improve the tracking performance. This is a limitation of the proposed method, even though the probability that the clutters have comparable amplitudes to the targets is low.

For statistical comparison, 100 MC runs are performed on exactly the same data using the CPHD filters with and without amplitude information. In order to evaluate the performance of the algorithms quantitatively, the optimal subpattern assignment (OSPA) metric is adopted [34]. When computing OSPA, we set the parameters, $p = 2$, $c = 5$ and $p = 2$, $c = 50$, and the average OSPA distances are shown in Figure 7. The results of Figure 7 show that by introducing the amplitude features, the amplitude-aid CPHD filter outperforms the conventional CPHD filter, attaining effective results with smaller miss distance.

## 5. CONCLUSION

Conventional CPHD filter discriminates targets from clutter only via the motion information, which is not reasonable in the situation of dense clutter. This paper first proposes an amplitude-aid CPHD filter for tracking multiple IR point targets. We use the prior knowledge of IR scene to build the imaging model of target and clutter, so our method can improve the tracking performance effectively. For further research, we can extend the amplitude-aid CPHD filter to multiple IR sensors tracking, especially in application of multi-band infrared sensor focal plane. Multi-band focal plane generates IR image that can be used in tracking without registration, which is very advantageous.

The amplitude-aid CPHD filter can also be extended to the situation of clustered target. A special example is group target tracking, which is also known as extended target tracking. Practically important examples are aircraft formations or ground moving convoys. FISST-based filters are important for extended/group target tracking. In the application of IR images, the amplitudes of the target are important pieces of information that can be incorporated into the FISST-based filters. But no such works have been carried out in the literature, so more researches need to be undertaken in future works.

## REFERENCES

1. De Visser, M., P. B. W. Schwering, J. F. de Groot, and E. A. Hendriks, "Passive ranging using an infrared search and track sensor," *Opt. Eng.*, Vol. 45, No. 2, 026402-1–026402-14, 2006.

2. Lampropoulos, G. A. and J. F. Boulter, "Filtering of moving targets using SBIR sequential frames," *IEEE Trans. Aerosp. Electron. Sys.*, Vol. 31, No. 4, 1255–1267, 1995.

3. Ender, T., R. F. Leurck, B. Weaver, et al., "Systems-of-systems analysis of ballistic missile defense architecture effectiveness through surrogate modeling and simulation," *IEEE Systems Journal*, Vol. 4, No. 2, 156–166, 2010.

4. Vo, B.-N., B.-T. Vo, N.-T. Pham, and D. Suter, "Joint detection and estimation of multiple objects from image observations," *IEEE Trans. Signal Process.*, Vol. 58, No. 10, 5129–5141, 2010.

5. Streit, R. L., M. L. Graham, and M. J. Walsh, "Multitarget tracking of distributed targets using histogram-PMHT," *Digital Signal Process.*, Vol. 12, Nos. 2–3, 394–404, 2002.

6. Fortmann, T., Y. Bar-Shalom, and M. Scheffe, "Sonar tracking of multiple targets using joint probabilistic data association," *IEEE J. Ocean. Eng.*, Vol. 8, No. 3, 173–184, 1983.

7. Pulford, G. W., "Taxonomy of multiple target tracking methods," *IEE Radar, Sonar and Navigation*, Vol. 152, No. 5, 291–304, 2005.

8. Zaveri, M. A., S. N. Merchant, and U. B. Desai, "Genetic IMM-NN based tracking of multiple point targets in infrared image sequence," *Lecture Notes in Computer Science*, Vol. 3285, 17–25, 2004.

9. Zaveri, M. A., S. N. Merchant, and U. B. Desai, "Robust neural-network-based data association and multiple model-based tracking of multiple point targets," *IEEE Trans. on Syst., Man, and Cybernetics — Part C: Applications and Reviews*, Vol. 37, No. 3, 337–351, 2007.

10. Song, T. L., D. Musicki, H. H. Lee, and X. Wang, "Point target probabilistic multiple hypothesis tracking," *IET Radar Sonar Navig.*, Vol. 5, 632–637, 2011.

11. Zaveri, M. A., S. N. Merchant, and U. B. Desai, "Multiple model based point targets tracking using particle filtering in infrared image sequence," *Opt. Eng.*, Vol. 45, No. 5, 184–189, 2004.

12. Zaveri, M. A., S. N. Merchant, and U. B. Desai, "Tracking of point targets in IR image sequence using multiple model based particle filtering and MRF data association," *Proceedings of the 17th International Conference on Pattern Recognition (ICPR'04)*, Vol. 4, 729–732, 2004.

13. Mahler, R. P. S., "Multi-target bayes filtering via first-order multi-target moments," *IEEE Trans. Aerosp. Electron. Sys.*, Vol. 39, No. 4, 1152–1178, 2003.

14. Mahler, R. P. S., "PHD filters of higher order in target number," *IEEE Trans. Aerosp. Electron. Sys.*, Vol. 43, No. 3, 1523–1543, 2007.

15. Vo, B.-T., B.-N. Vo, and A. Cantoni, "Analytic implementations of the cardinalized probability hypothesis density filtering," *IEEE Trans. Signal Process.*, Vol. 55, No. 7, 3553–3567, 2007.

16. Mahler, R., *Statistical Multisource-multitarget Information Fusion*, Artech House, Norwood, MA, 2007.

17. Vo, B.-T., B.-N. Vo, and A. Cantoni, "The cardinality balanced multitarget multi-bernoulli filter and its implementations," *IEEE Trans. Signal Process.*, Vol. 57, No. 2, 409–423, 2009.

18. Lerro, D. and Y. Bar-Shalom, "Interacting multiple model tracking with target amplitude feature," *IEEE Trans. Aerosp. Electron. Sys.*, Vol. 29, No. 2, 494–508, 1993.

19. Brekke, E., O. Hallingstad, and J. Glattetre, "Tracking small targets in heavy-tailed clutter using amplitude information," *IEEE J. Ocean. Eng.*, Vol. 35, No. 2, 314–329, 2010.

20. Brekke, E., O. Hallingstad, and J. Glattetre, "The modified riccati equation for amplitude-aided target tracking in heavy-tailed clutter," *IEEE Trans. Aerosp. Electron. Sys.*, Vol. 47, No. 4, 2874–2886, 2011.

21. Van Keuk, G., "Multi-hypothesis tracking using incoherent signal-strength information," *IEEE Trans. Aerosp. Electron. Sys.*, Vol. 32, No. 3 1164–1170, 1996.

22. Xu, Y., H. Xu, W. An, and D. Xu, "FISST based method for multi-target tracking in the image plane of optical sensors," *Sensors*, Vol. 12, 2920–2934, 2012.

23. Clark, D., B. Ristic, B. Vo, et al., "Bayesian multi-object filtering with amplitude feature likelihood for unknown object SNR," *IEEE Trans. Signal Process.*, Vol. 58, No. 1, 26–37, 2010.

24. Gunapala, S. D., S. V. Bandara, et al., "Demonstration of megapixel dual-band QWIP focal plane array," *IEEE J. Quantum Elect.*, Vol. 46, No. 2, 285–293, 2010.

25. Price, S., W. Ritchie, E. Schulte, R. Wyles, et al., "Staring $256 \times 256$ LWIR focal plane array performance of the Raytheon exoatmospheric kill vehicle," ADA Report, 1998.

26. Chan, D. S. K., D. A. Langan, and D. A. Staver, "Spatial processing techniques for the detection of small targets in IR clutter," *Proc. SPIE*, Vol. 1305, 53–62, 1990.

27. Gascon, F., J.-P. Gastellu-Etchegorry, and M.-J. Lefêvre, "Radiative transfer model for simulating high-resolution satellite images," *IEEE Trans. Geosci. Remote Sensing*, Vol. 39, No. 9, 1922–1926, 2001.

28. Zhao, F., H. Lu, and Z. Zhang, "Real-time single pass connected components analysis algorithm," *EURASIP Journal on Image and Video Processing*, Vol. 2013, No. 1, 1–10, 2013.

29. Kay, S. M., *Fundamentals of Statistical Signal Processing, Volume 1: Estimation Theory*, Prentice Hall, PTR Upper Saddle River, New Jersey, 1993.

30. Mahler, R. P. S., "Multi-target Bayes filtering via first-order multi-target moments," *IEEE Trans. Aerosp. Electron. Sys.*, Vol. 39, No. 4, 1152–1178, 2003.

31. Mahler, R. P. S., "PHD filters of higher order in target number," *IEEE Trans. Aerosp. Electron. Sys.*, Vol. 43, No. 3, 1523–1543, 2007.

32. Mahler, R. P. S., *Statistical Multisource Multitarget Information Fusion*, Artech House, Norwood, MA, 2007.

33. Vo, B.-N. and W.-K. Ma, "The Gaussian mixture probability hypothesis density filtering," *IEEE Trans. Signal Process.*, Vol. 54, No. 11, 4091–4104, 2006.

34. Ristic, B., B.-N. Vo, D. Clark, and B.-T. Vo, "A metric for performance evaluation of multitarget tracking algorithms," *IEEE Transactions on Signal Processing*, Vol. 59, No. 7, 3452–3457, 2011.